Construction of microelectronic nanostructures and nanodevices using polyoxometallates

Dimitrios Velessiotis[*]
National and Kapodistrian University of Athens
Department of Informatics and Telecommunications,
Institute of Microelectronics, NCSR Demokritos

Abstract. The use of tungsten polyoxometalates (with main representative in this work the phosphotungstic acid $H_3[PW_{12}O_{40}]$) for the construction of molecular nanodevices is explored in this work. For this purpose, the electrical behavior of polyoxometalate containing materials was studied as well as the possibility of using such materials in pattern-transfer procedures, such as the electron beam lithography. Metal-Insulator-Metal (MIM) junctions were studied during the electrical characterization of polyoxometalate-containing materials. The insulating part of such devices was a polymeric film containing the phosphotungstic anion $[PW_{12}O_{40}]^{3-}$. Vertical structures, either with or without a SiO_2 layer between the polyoxometalate layer and one of the metallic electrodes, were also studied. In spite of the fact that the materials used presents ageing phenomena, it became clear that $H_3[PW_{12}O_{40}]$ possesses the needed conductivity in order to be used in nanometer-scale molecular devices. In addition, the lithographic study of polyoxometalate-containing materials showed the possibility of a reliable electron beam lithography procedure in the nanometer scale, both for a positive and a negative tone material. The experimental study was completed by the development of a Monte Carlo electron beam lithography simulation program. The accurate relations for the electron elastic scattering for both the high and low energy region are implemented in this program, so that it can be used in high and low voltage electron beam lithography.

Keywords: molecular electronics, Polyoxometalates, Monte-Carlo simulation, electron-beam lithography, metal-insulator-metal (MIM) junctions, current-voltage (I-V) characteristics.

1 Introduction

The gigantic growth of Microelectronics industry is mainly owed to the continuous miniaturization of metal-oxide-semiconductor field-effect transistor (MOSFET) - a fact known as Moore s law [1]. According to the International Technology Roadmap for Semiconductors [2], continuing this course will eventually come to an end at best during the 2020 s decade, due to the fact that MOSFET s physical gate length will be 7nm. With MOSFET s dimensions approaching the atomic scale a number of different devices (e.g. [3-7]) and/or concepts [8-11] were

[*] Dissertation Advisor: Angela Arapoyanni, Assoc. Professor

introduced in order to supplement MOSFET and prepare the next era of microelectronics. As circuit dimensions have already approached the atomic scale, the use of Chemistry and Material Science, in order to provide us with molecules or materials with the ability to perform logical calculations [12] or present memory effect [13], is a tempting idea. However, there is a long way before we can use molecular systems as logical or storage elements. Both procedures and materials which will be used to implement this idea should be found from scratch, a situation posing difficult to answer technological as long as theoretical problems to the researchers who are dealt with it.

The use of phosphotungstic acid ($H_3PW_{12}O_{40}$-POM) in molecular electronic systems is studied, for the first time, within this work. The lithographic performance [14-16] as well as, the electrical properties [16-21] of materials based on POM is investigated, so that both the material needed and the procedures for patterning it are obtained.

2 Experimental results and discussion

2.1 Electrical characterization

In order to study the electrical properties of the materials concerned, aluminum or gold planar electrodes separated 20-500 nm apart were fabricated on SiO_2 using a standard PMMA lift-off process and electron-beam lithography. Two different electrode configurations have been used: (a) one in the shape of opposing fingers with a nanometer distance [18] and (b) another in the shape of parallel lines with nanometer interspacing (Fig. 1). The second configuration has the advantage of allowing for homogeneous electric fields and larger currents in the interspace and therefore more stable measurements. The opposite finger geometry results in more intense fields for a given applied voltage and smaller currents. Furthermore, since the number of active molecules between the electrodes is generally smaller than in the case of long parallel electrodes, the appearance of quantum tunnelling effects is favored although transport is more sensitive to the fluctuation of the number of molecules. The results presented here (unless noted otherwise) are based on measurements with parallel electrodes. A layout of the structures used for the electrical measurements is shown in Fig. 1.

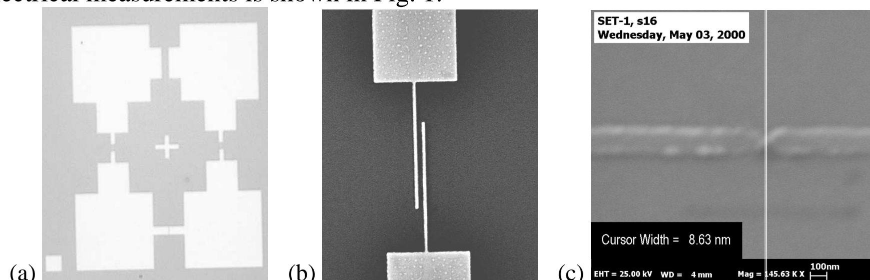

Fig. 1. E-beam fabricated parallel electrodes on 200 nm SiO2 over Si. (a) General view. (b) parallel lines configuration (c) opposite finger geometry.

In a search for a suitable polymer matrix, it should be considered that the host material should not react with the embedded molecules, thus altering their transport properties, and at the same time the composite material should preferably behave as a lithographic resist with nanometer resolution for nanofabrication process simplification reasons. Poly (methyl methacrylate) (PMMA) meets both demands. Solutions of POM and high molecular weight PMMA into PGMEA solvent were prepared. The relative concentration of POM/PMMA was varied in the range 1:4 w/w up to 5:1 w/w.

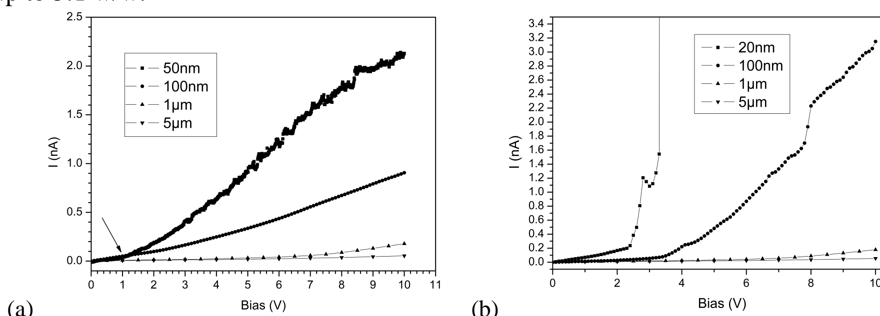

Fig. 2. Current vs voltage graph, in the case of the 5 over 1 (POM/PMMA) material for various distances and planar (a) Al electrodes: The abrupt current change found at 50 nm distant electrodes (indicated by an arrow) disappears in greater distances. (b) Au electrodes: The absence of natural oxide underlines the observed effects.

In order to study the transport characteristics and single out the tunneling effects of these composite systems, the electrode distance, the electrode material, and the molecular concentration were treated as variable parameters. In Fig. 2a, a typical result with Al electrodes is shown. In the case of interelectrode distances larger than 50 nm the behavior is approximately Ohmic with the exception of a small nonlinear region for voltages lower than 1 V. This Ohmic behaviour is due to hopping conductivity through tungstate molecules which, in our case, are 2.25 nm apart. Since the molecular size is 1-1.5 nm the net distance between molecules is estimated to be 0.75-1.25 nm in this concentration. In the case of small interelectrode distance (L=50 nm), a nonlinear conductivity change appears. This change suggests a saturation effect, i.e., the transition from the barrier-limited conduction to the bulk-limited conduction dominated by hoping transport. In order to investigate this effect and distinguish the part that is due to the insulating PMMA matrix, structures with Au electrodes were also tested (Fig. 2b). The nonlinear conductivity change still appears, which is evidence of the fact that it is mainly dependent on the material, rather than on the electrode. In the case of the 20 nm gold electrodes strong oscillations appear after 2.5 V. Comparing the results in the case of Al and Au electrodes it is deduced that the barrier appears for smaller electrode distances in both cases. Effects are less dramatic in the case of Al electrodes due to the presence of the natural oxide, which has a high contribution in the case of lower voltages. We have checked electrode distances as low as 10 nm obtaining qualitatively the same results. In the case of such small distances only a few molecules are aligned in the direction of the electric field.

For example, in the case of a 1:1 w/w concentration and D nm electrode distance, the mean distance between molecules is <d>=3 nm resulting in 3-4 molecules along the field. The electrons reach the molecules through the PMMA insulating barrier undergoing multiple tunneling. The band alignment between electrodes and molecular levels becomes important in this extreme case. An alignment scheme is shown in Fig. 3 based on published data for tungstate POMs [22]. Although the Fermi levels for Al and Au are positioned above and lower than the LUMO level, respectively, the effect on a two-electrode metal insulator metal (MIM) device should be similar due to symmetry. The currents observed in the case of Au electrodes are higher.

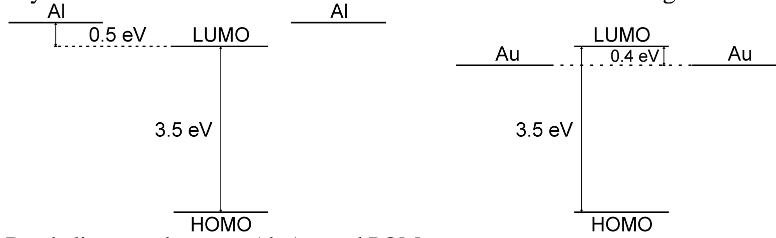

Fig. 3. Band alignment between Al, Au, and POM.

Since the main mechanism between molecules in an insulating environment is hopping conductivity, current depends strongly on the molecular content of the composite material. Decreasing the molecular concentration results in lower currents and, in the case of parallel finger electrodes, the disappearance of the current discontinuity. This result should be compared with results where opposite finger electrodes were used. The higher electric field developed between the opposite electrodes resulted in higher currents and the dramatically smaller number of molecules involved resulted in the appearance of abrupt current changes even in the case of 1:1 w/w concentration.

In the case of nanometer distant electrodes the I-V characteristic may be divided into three parts: (a) the low-voltage region, (b) the region around the abrupt current change (Fowler Nordheim region), and (c) the space-charge-limited region. In the case of low-bias voltages, tunneling mechanisms dominate transport. A detailed theoretical model in this case should take into account both tunneling through the metal barriers as well as multiple tunneling between the molecules. However a simple tunneling model through a MIM structure provides a good fit of the experimental results. In the present paper we discuss the low-voltage part of the I-V characteristic in terms of the analytical expression derived by Simmons [23], which describes tunneling through a MIM structure with a thin insulating barrier of length d:

$$I = I_0 \times \left\{ \Phi \times \exp\left(-a\sqrt{\Phi}\right) - \left(\Phi + eV\right) \times \exp\left(-a\sqrt{\Phi + eV}\right) \right\} \qquad \textbf{(0)}$$

where:

$$a = 2d\frac{\sqrt{2m}}{h} \qquad \textbf{(2)}$$

, d is the film thickness, m is the electron mass, and Φ is the mean barrier height for the whole system. (1) includes both the contact effects as well as the insulating

barriers between molecules. A straightforward least-squares fitting of experimental data to (1) presents convergence difficulties due to the presence of the three parameters, Φ, I_0 and d. To avoid these difficulties, the data are first extrapolated with the use of a third power law $I=c1 \cdot V + c2 \cdot V^2 + c3 \cdot V^3$, and then the coefficients c1, c2, c3 are identified with the corresponding coefficients resulting from the Taylor expansion of (1). The resulting nonlinear system for Φ, I_0 and d is solved numerically and a unique solution is always established. This first set of parameters serves as initial values for accurate nonlinear regression analysis. The results are demonstrated in Fig. 4. Φ calculated from the low-voltage data region depends mostly upon the device geometry and the POM concentration of the materials, and less upon the electrode material. In the case of a 1:1 w/w concentration and electrode distance 20-50 nm, Φ=0.65eV. The potential entering (1) is actually a mean value with contributions both from the interfaces and the material. The Fowler Nordheim region analysis allows the evaluation of the material contribution for the barrier potential. For example, in the case of 1:1 w/w concentration Φ_{FN}=0.39eV using the data of Fig. 5.

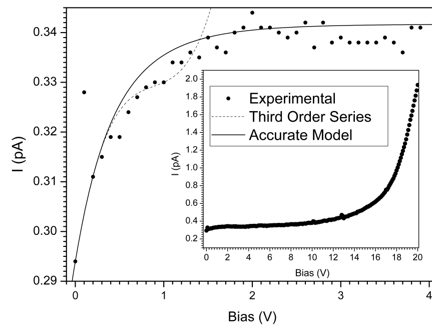

Fig. 4. Analysis of the low-voltage region of the I-V characteristics (normal graph) and the original data (nested graph). The specific sample was made of the 1 over 1 material spun on Al electrodes.

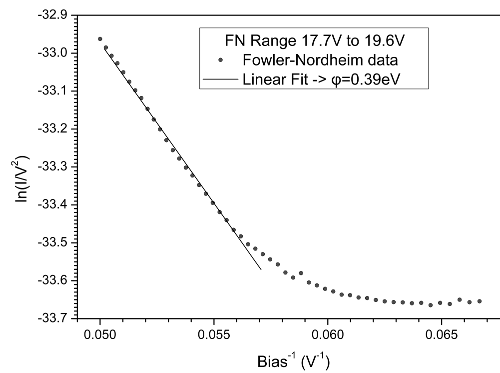

Fig. 5. Fowler Nordheim plot of the data of Fig. 4. The calculated barrier height was 0.39 eV.

Low-temperature experiments using a nitrogen cryostat were performed in order to investigate the temperature dependence of the conductance. Conductivity follows an Arrhenius law revealing a hopping mechanism with activation energy E_0=0.12±0.01eV in the case of the 1:5 w/w concentration. This activation energy is

quite small and provides a physical basis for the explanation of transport via a hopping mechanism.

Similar results were obtained with the PHECIMA/POM formulation, which was tested before the PMMA/POM one. It was proved though [22] that PHECIMA reacts with POM, failing to comply with the specifications mentioned above. Vertical structures, either with or without a SiO_2 layer between the POMe layer and one of the metallic electrodes, were also studied. A typical capacitance measurement in a Al/ n+ Si/SiO_2/POM-PMMA/Al stack is given in Fig. 6.

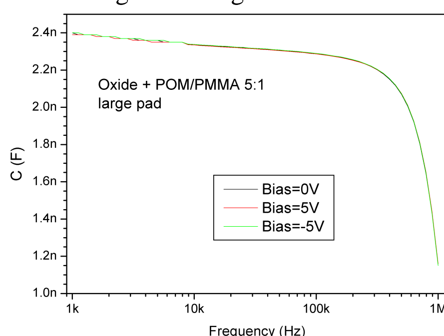

Fig. 6. Capacitance vs. frequency graph in a Al/n+ Si/SiO2/POM-PMMA/Al vertical device.

2.2 Electron Beam Lithography - Experimental

A successful material for molecular applications, apart from satisfying conductivity, should allow the patterning of the active molecular channel in a direct manner without using additional resist processing. So, it is rather straightforward to test different formulations of POM/lithographic resist mixtures, targeting at a combination of successful lithography and a stable final material after processing. There were two successful formulations in respect with their lithographic performance: (a) Poly(vinyl alcohol) (PVA) based formulations and (b) PMMA/POM.

PVA based formulations, very similar to the ones that had been used in the past [24], were first evaluated as e-beam negative lithographic resists. The polymer that gave best results had been purchased by Fluka (Mw 22,000 and degree of hydrolysis 98.5 %) and used without further purification. A formulation containing 4.3 % w/w PVA and 14.4 % w/w $H_3PW_{12}O_{40}$ in water was selected for bilayer e-beam lithography. This material was very close to the one used before for optical and X-ray lithography [24] and for this reason the thermal processing and development conditions were also kept close to the ones reported there: Pre-exposure bake 70°C for 1 min, Post exposure bake 80°C for 1-2 min, Development with acidic aqueous solutions (Developer 2M H_3PO_4/0.02M $H_3PW_{12}O_{40}$, rinser 3M HCl). Hard baked novolac was used as the bottom layer and the pattern was transferred to this layer with a suitable two step oxygen plasma process: 8 sec O_2/SF_6 (9:1) followed by 140 sec O_2. In this process the polyoxometallate compound serves as the oxygen plasma resistant additive. The first step was used in order to remove any polyoxometallate residues from the developed regions, which would cause micromasking and thus inefficient pattern transfer. The sensitivity obtained was quite good (10-50 μC/cm^2) as expected

by the presence of relatively high percentage of W in their composition, and despite the low amplification imaging chemistry in these systems [19]. On the other hand the demanding process limited the quality of the obtained lithographic features, especially due to the need for aggressive etching steps that resulted in high roughness. Nevertheless, isolated lines of less than 80nm were received with this type of materials as demonstrated in Fig. 7.

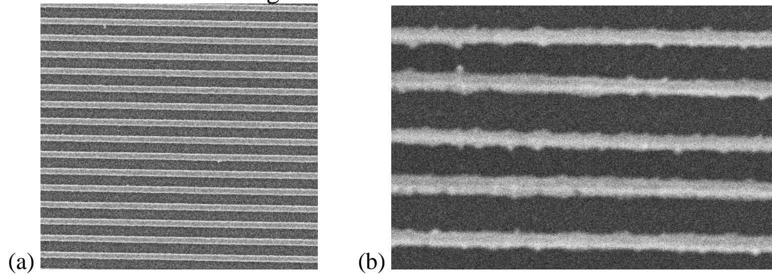

Fig. 7. (a) Dense 500nm lines (50μC/cm^2) and (b) isolated 80nm lines (32μC/cm^2) on polyoxometallate containing PVA electron beam resist after etching. E-beam energy was 50keV. The line profile was obtain after etching.

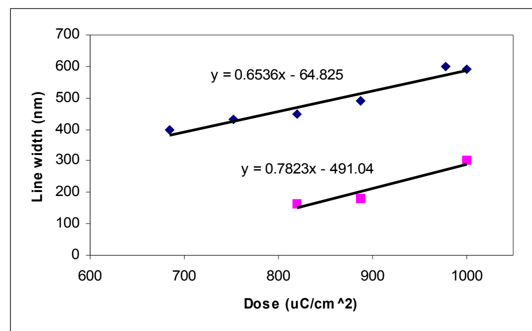

Fig. 8. Line width vs. dose in the case of PMMA/Tungstate formulation in the case of dense 200nm and 500nm lines. The line width variation is limited to 8nm for a 1% dose variation.

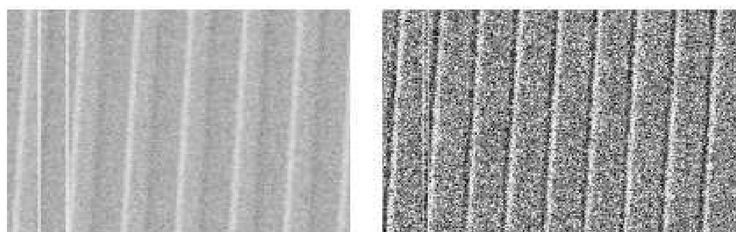

Fig. 9. Dense 500nm (887 μC/cm2) lines and isolated 60nm lines (920 μC/cm2) patterned by 50keV e-beam lithography on a PMMA/Tungstate formulation.

Positive materials were formulated based on PMMA and POMs. In this case imaging with e-beam was based on the well known PMMA chain scission chemistry. Conventional PMMA processing was used as well. The unexposed part of the film in this case seemed intact after the development and spectroscopic studies showed that

the POM content in the film was not reduced. Thus, the most serious problem encountered in the negative systems, which led to the use of unconventional acidic developers, was not encountered here. Dense and isolated lines in the range 50-500nm where written at 50keV and the optimal dose was searched for in each case. It was proved that generally the dose required for high resolution lines was about 30% higher than for pure PMMA resists. This is attributed to the fact that a considerable part of the incident energy is absorbed in the excitation of the polyoxometallates, thus not contributing to PMMA chemistry. On the other hand the presence of polyoxometallates in the PMMA film enhances etch resistance, therefore thinner resist films suitable for high resolution patterning and effective pattern transfer are possible. From the linewidth vs. dose diagram shown in Fig. 8 it may be deduced that 1% dose variation results in a variation of the linewidth by 7-8nm, providing an excellent process window for the resist. High resolution lines of 60nm are demonstrated in the right part of Fig. 9.

2.3 Electron Beam Lithography - Simulation

Microcolumn electron beam lithography was considered at the beginning of the millennium among the candidates for the production of future generation sub-100nm devices. Use of low energies, in the 100 2000eV range, calls for new lithographic techniques involving thin films of thickness less than 100 nm and surface imaging methods. An electron beam lithography simulator is required in order to support experimental work in this region. A simulator based on earlier techniques based on the well-known Partial Wave Expansion Method (PWEM) [25] is presented here. In contrary with previous approaches (e.g. [26]) though, all cross sections are evaluated in detail avoiding the use of semi-empirical relations.

Fig. 10. Energy Deposition function for a 50 nm oxometalate film over an Si substrate.

The first step is to evaluate the differential cross section in the energy range 100 2000 eV and compare the results to those obtained by the Born approximation. The difference in the case of 1000 eV is small and it is limited to large angle scattering. However, the differences are significant in the case of the oxometalate resist. It is obvious that the Born approximation is not successful even for small angle scattering events. This scattering cross section is used by the Monte-Carlo code to evaluate the energy deposition function (EDF) inside the resist film. The EDF was evaluated in the case of PMMA films of 50 and 100 nm thickness over Si in the case of e-beam energies in the range of 100 2000 eV. In Fig. 10, the PWEM is compared to the Born approximation in the case of a 50-nm polyoxometalate resist film over Si. It is obvious that although the Born cross sections are quite different than those obtained with the PWEM, the EDF is not significantly different.

The PSF is used as an input to the simulation tool SELID in order to obtain the final developed profiles of the resist films. The PSF is convoluted in order to obtain a real beam with point size 5nm. Results are demonstrated in the case of 1keV in Fig. 11. In agreement with experimental data [27], energy of 1keV is adequate for the exposure of a 50-nm PMMA film. Due to the large angle scattering in the case of the oxometalate resist the deviation from the vertical of the line patterns is significant.

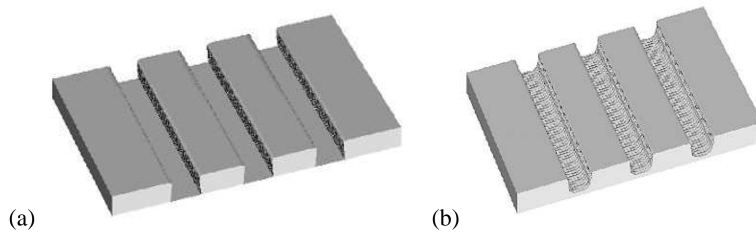

Fig. 11. Final developed profiles obtained from the SELID simulator for beam energy of 1keV (a) 50-nm PMMA film and (b) 50-nm POM film.

3 Conclusions

Transport properties as well as lithographic performance of polyoxometalate containing materials were presented in this work. The adequate conductivity shown by most of the formulations studied as long as the ability for pattern transfer, advocates for continuing the work to the direction of using the materials in future molecular devices.

References

1. Moore, G., Cramming more components onto integrated circuits, Electronics 38, 114 (1965)
2. International Technology Roadmap for Semiconductors 2005 ed. (ITRS 2005), Executive Summary, page 63
3. Tans, S.J., Verschueren, A.R.M. and Dekker, C., Room-temperature transistor based on a single carbon nanotube, Nature 393, 49 (1998)
4. Huang, Y., Duan, X., Wei, Q. and Lieber, C.M., Directed Assembly of One-Dimensional Nanostructures into Functional Networks, Science 291, 630 (2001)
5. Brokaert, T.P.E., Lee, W. and Fonstad, G., Pseudomorphic $In_{0.53}Ga_{0.47}As$/AlAs/InAs resonant tunneling diodes with peak-to-valley current ratios of 30 at room temperature, Appl. Phys. Lett. 53, 1545 (1988)
6. Dorojevets, M., An 8-bit FLUX-1 RSFQ microprocessor built in 1.75-μm technology, Physica C: Superconductivity, 378-381, 1446 (2002)
7. Likharev, K. K., Single-Electron Devices and Their Applications, IEEE Proc. 87, 606 (1999)
8. Lent, C. S., Tougaw, P. D. and Porod, W., Bistable saturation in coupled quantum dots for quantum cellular automata, Appl. Phys. Lett. 62, 714 (1993)
9. Toth, G., Lent, C. S., Tougaw, P. D., Brazhnik, Y., Weng, W., Porod, W., Liu, R.-W. and Huang, Y.-F., Quantum cellular neural networks, Superlattices and Microstructures 20, 473 (1996)
10. Adleman, L.M., Molecular Computation of Solutions To Combinatorial Problem, Science 266, 1021 (1994)
11. Georgeot, B., Quantum computing for physics research, Nuclear Instruments and Methods in Physics Research A 559, 6 (2006)
12. Aviram, A. and Ratner, M. A., Molecular rectifiers, Chem. Phys. Lett. 29, 277 (1974)

13. Ma, L.P., Liu, J. and Yang, Y., Organic electrical bistable devices and rewritable memory cells, Appl. Phys. Lett., 80, 2997 (2002)
14. Zianni X., Velessiotis D., Glezos N. and Trohidou K.N., Application of the Partial Wave Expansion Method in 3-D Low Energy Electron Beam Lithography Simulation, Microel. Eng., 57-58, 297 (2001)
15. Velessiotis D., Zianni X., Glezos N. and Trohidou K.N., Development of a new low energy electron beam lithography simulation tool, Proc. of Microelectronics, Microsystems and Nanotechnology (MMN 2000), p.147
16. Glezos N., Argitis P., Velessiotis D., Koutsolelos P., Diakoumakos C.D., Tserepi A. and Beltsios, K., Polyoxometallate containing polymeric materials for nanolithography and molecular devices (Invited), MRS Fall Online Proc. 705, Y2.5 (2001)
17. Glezos N., Velessiotis D., Chaidogiannos G., Argitis P., Tsamakis D. and Zianni X., Transport properties of polyoxometalate containing polymeric materials, Synth. Metals 138, 267 (2003)
18. Glezos N., Argitis P., Velessiotis D. and Diakoumakos C.D., Tunneling Transport in Polyoxometallate Composite Materials, Appl. Phys. Lett. 83, 488 (2003)
19. Chaidogiannos G., Velessiotis D., Argitis P., Koutsolelos P, Diakoumakos C.D., Tsamakis D. and Glezos N., Tunneling and Negative Resistance Effects for composite Materials Containing Polyoxometallate Molecules, Microel. Eng. 73-74, 746 (2004)
20. Velessiotis D., Glezos N. and Ioannou-Sougleridis V., Tungstate polyoxometalates as active components of molecular devices, J. Appl. Phys. 98, 084503 (2005)
21. Velessiotis D., Chaidogiannos G., Glezos N. Argitis P. and Tsamakis D, Quantum effects in molecular nanodevices based on tungsten polyoxometalates, Proc. Of 3rd European Microelectronics and Packaging Symposium (EMPS), Prague 16-18 June 2004, pp. 221-226
22. Hiskia, A., Mylonas, A. and Papaconstantinou, E., Comparison of the photoredox properties of polyoxometallates and semiconducting particles, Chem. Soc. Rev. 30, 62 (2001)
23. Simmons, J. G., Generalized Formula for the Electric Tunnel Effect between Similar Electrodes Separated by a Thin Insulating Film, J. Appl. Phys. 34, 1793 (1963)
24. Carls, J. C., Argitis, P. and Heller, A., Deep Ultraviolet Photoresist Based on Tungsten Polyoxometalates and Poly(Vinyl Alcohol) for Bilayer Photolithography, J. Electrochem. Soc. 139, 786 (1992)
25. Czy~ewski, Z., O Neill-MacCallum, D., Romig, A. and Joy, D. C., Calculations of Mott scattering cross section, J. Appl. Phys. 68, 3066 (1990)
26. Kim, S.-H., Ham, H.-M., Lee, W. and Chun, K., New approach of Monte Carlo simulation for low energy electron beam lithography, Microel. Eng. 41-42, 179 (1998)
27. Olkhovets, A. and Craighead, H. G., Low voltage electron beam lithography in PMMA, J. Vac. Sci. Technol. B 17, 1366 (1999)